Journal of Power Sources 186 (2009) 311–319

Contents lists available at ScienceDirect

Journal of Power Sources

journal homepage: www.elsevier.com/locate/jpowsour

Synthesis and characterization of carbon dioxide and boiling water stable proton conducting double perovskite-type metal oxides

Surinderjit Singh Bhella, Venkataraman Thangadurai*

Department of Chemistry, University of Calgary, 2500 University Dr. NW, Calgary, AB T2N 1N4, Canada

ARTICLE INFO

Article history:
Received 4 September 2008
Received in revised form
28 September 2008
Accepted 30 September 2008
Available online 11 October 2008

Keywords:
Ceramic proton conductors
Double perovskites
Chemical stability
Ta-doped $Ba_2(Ca,Nb)_2O_6$
AC impedance
X-ray diffraction

ABSTRACT

In this paper, we report the synthesis, chemical stability and electrical properties of three new Ta-substituted double perovskite-type $Ba_2Ca_{2/3}Nb_{4/3}O_6$ (BCN). The powder X-ray diffraction (PXRD) confirms the formation of double perovskite-like structure $Ba_2(Ca_{0.75}Nb_{0.59}Ta_{0.66})O_{6-\delta}$, $Ba_2(Ca_{0.75}Nb_{0.66}Ta_{0.59})O_{6-\delta}$ and $Ba_2(Ca_{0.79}Nb_{0.66}Ta_{0.55})O_{6-\delta}$. The PXRD of CO_2 treated (800 °C; 7 days) and water boiled (7 days) samples remain the same as the as-prepared samples, suggesting a long-term structural stability against the chemical reaction. The electrical conductivity of the investigated perovskites was found to vary in different atmospheres (air, dry N_2, wet N_2, H_2 and $D_2O + N_2$). The AC impedance investigations show bulk, grain-boundary and electrode contributions in the frequency range of 0.01 Hz to 7 MHz. Below 600 °C, the bulk conductivity in wet H_2 and wet N_2 was higher than in air, dry H_2 and dry N_2. However, an opposite trend was observed at high temperatures, which may be ascribed to p-type electronic conduction. The electrical conductivity of the investigated perovskites was decreased in $D_2O + N_2$ compared to that of $H_2O + N_2$ atmosphere. This clearly shows that the investigated Ta-doped BCN compounds exhibit proton conduction in wet atmosphere which was found to be consistent with water uptake. The water uptake was further confirmed by thermogravimetric analysis (TGA) and Fourier transform infrared spectroscopy (FTIR) characterization. Among the samples investigated, $Ba_2(Ca_{0.79}Nb_{0.66}Ta_{0.55})O_{6-\delta}$ shows the highest proton conductivity of 4.8×10^{-4} S cm^{-1} (at 1 MHz) at 400 °C in wet (3% H_2O) N_2 or H_2, which is about an order of magnitude higher than the recently reported 1% Ca-doped $LaNbO_4$ at the same atmosphere and at 10 kHz.

Crown Copyright © 2008 Published by Elsevier B.V. All rights reserved.

1. Introduction

Current progress in proton exchange membrane fuel cells (PEMFCs) technology is mainly based on perfluorocarbon sulfonic acid polymer electrolyte (Nafion) and Pt–C electrodes, which operates efficiently at about 80 °C [1]. However, problems with the commercialization of Nafion-based PEMFCs include water management (to retain high proton conductivity), CO poisoning and high costs of Pt electrodes, and crossover of fuels (e.g., CH_3OH) [2,3]. As a result, high temperature (above 100 °C) polymer and or ceramic membranes are being investigated to overcome these problems. Furthermore, high operating temperature PEMFCs have the advantage of increasing the kinetics of electrode reactions, being more tolerant towards CO poisoning as well as enhancing the proton conductivity of the membranes [4–6].

Two approaches were considered to replace Nafion in the conventional PEMFCs. The first strategy involves development of thermally stable organic–inorganic polymers, using fluoropolymers, polysiloxanes and phenylene backbones [4–8]. The second tactic involves the development of solid-state proton conductors (SSPCs) based on inorganic metal oxides and composite materials [9–14]. Based on temperature, SSPCs are classified into mainly two categories: (i) low-temperature (LT) and (ii) high-temperature (HT) proton conductors. Typical examples of LT-SSPCs include $HUO_2PO_4{\cdot}4H_2O$, $CsHPO_4$, and $H_3PW_{12}O_{40}{\cdot}nH_2O$ ($n = 30$), which are unstable at high temperature and therefore limit their applications in HT PEMFCs. Acceptor doped perovskite-type ABO_3 (A = Sr, Ba, B = Ce, Zr) are some of the well-known examples for the HT-SSPCs [15,16]. The origin of proton conduction in the HT-SSPCs was investigated intensively by many authors [10,15–19], and it has been established that the conduction occurs by means of the defect equilibrium reactions between the oxygen vacancies ($V_O^{\bullet\bullet}$), lattice oxygen (O_O^x) and H_2O vapour at elevated temperatures, i.e.,

$$H_2O_{(g)} + V_O^{\bullet\bullet} + O_O^x \rightarrow 2OH_O^{\bullet} \quad (1)$$

(where $OH_O^{\bullet}$ represents a proton attached to a lattice oxygen).

Among the HT-SSPCs reported, so far, Y_2O_3-doped $BaCeO_3$ (BCY) shows good proton conductivity in humidified H_2. However, several

* Corresponding author. Tel.: +1 403 210 8649.
E-mail address: vthangad@ucalgary.ca (V. Thangadurai).

0378-7753/$ – see front matter. Crown Copyright © 2008 Published by Elsevier B.V. All rights reserved.
doi:10.1016/j.jpowsour.2008.09.110

Table 1
Indexed PXRD data of $Ba_2(Ca_{0.79}Nb_{0.66}Ta_{0.55})O_{6-\delta}$.

h	*k*	*l*	as-prepared			CO_2 treated			H_2O treated		
			$d_{(obs.)}$ (Å)	$d_{(calc.)}$ (Å)	$I_{(obs.)}$ (%)	$d_{(obs.)}$ (Å)	$d_{(calc.)}$ (Å)	$I_{(obs.)}$ (%)	$d_{(obs.)}$ (Å)	$d_{(calc.)}$ (Å)	$I_{(obs.)}$ (%)
1	1	1	4.8055	4.8340	7	4.8127	4.8350	6	4.8076	4.8427	8
2	0	0	4.1684	4.1864	2	4.1719	4.1872	2	4.1676	4.1939	3
2	2	0	2.9531	2.9602	100	2.9550	2.9608	100	2.9569	2.9655	100
3	1	1	2.5197	2.5245	4	2.5212	2.5250	3	2.5226	2.5290	3
2	2	2	2.4138	2.4170	7	2.4150	2.4175	7	2.4175	2.4213	8
4	0	0	2.0906	2.0932	30	2.0915	2.0936	31	2.0943	2.0969	29
3	3	1	1.9193	1.9208	2	1.9202	1.9212	2	1.9233	1.9243	2
4	2	0	1.8702	1.8722	2	1.8718	1.8725	2	1.8748	1.8756	2
4	2	2	1.7084	1.7090	41	1.7090	1.7094	39	1.7113	1.7121	33
5	1	1	1.6112	1.6113	2	1.6112	1.6116	2	1.6142	1.6142	2
4	4	0	1.4801	1.4801	20	1.4805	1.4804	15	1.4827	1.4828	15
5	3	1	1.4154	1.4152	2	1.4158	1.4155	2	1.4177	1.4178	2
6	0	0	1.3959	1.3954	2	–	–	–	–	–	–
6	2	0	1.3245	1.3238	16	1.3245	1.3241	14	1.3267	1.3262	13
6	2	2	1.2633	1.2622	2	1.2632	1.2625	2	1.2653	1.2645	2
4	4	4	1.2092	1.2085	5	1.2097	1.2087	5	1.2117	1.2107	4
				$a = 8.373(2)$ Å			$a = 8.374(2)$ Å			$a = 8.388(2)$ Å	

problems exist with regards to the applications of BCY in PEMFCs due to its poor chemical stability in CO_2 containing atmospheres and in high levels of humidity [10–13,20–24]. Haile and coworkers [25] and other [26,27,28] claimed that the partial replacement of Ce by Zr in BCY was found to improve the chemical stability in CO_2, but, the electrical conductivity decreases with increasing Zr content in BCY [27,28]. Furthermore, the Zr-doped BCY exhibits poor mechanical stability and high grain-boundary resistance [11,12,29–31] and hence limits its practical application in PEMFCs.

Nowick et al. [32–35] and several others [36–42] investigated the proton conductivity of non-stoichiometric double perovskite-type structure $Ba_2Ca_{2/3}Nb_{4/3}O_6$ (BCN). In the present work, we show that partial substitution of Ta for Nb in BCN yields, novel proton conductors, which exhibit a long-term chemical stability in CO_2 at elevated temperature and in boiling H_2O for 7

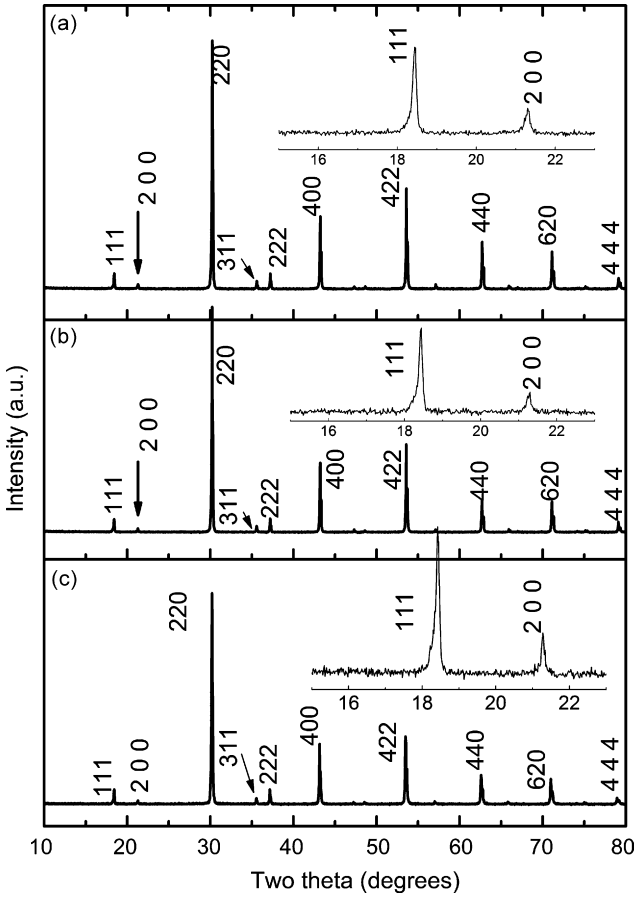

Fig. 1. Powder X-ray diffraction patterns of $Ba_2(Ca_{0.79}Nb_{0.66}Ta_{0.55})O_{6-\delta}$ (a) as-prepared, (b) sample 'a' heated in 100% CO_2 at 800 °C for 7 days, and (c) sample 'a' heated in boiling water for 7 days. Insets show the selected area PXRD.

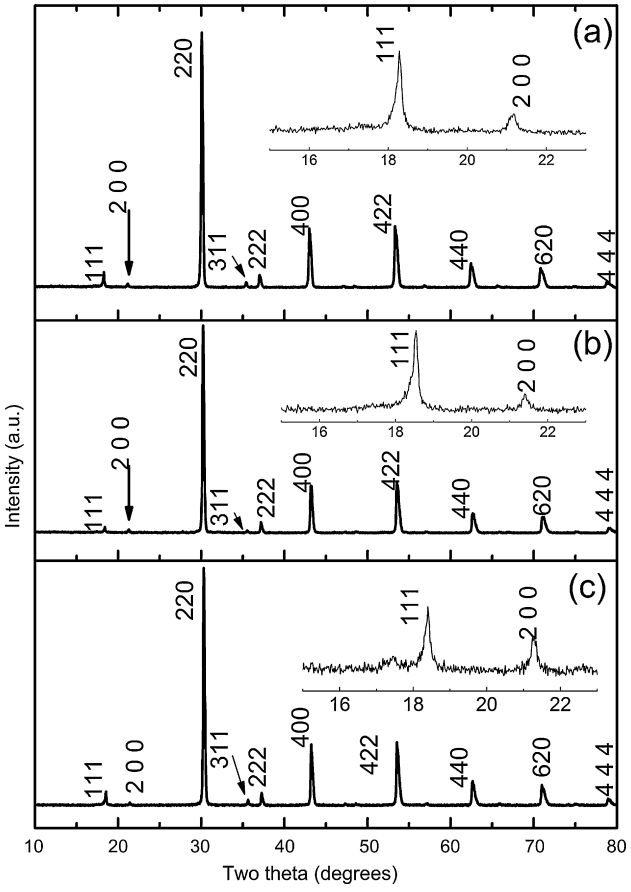

Fig. 2. Powder X-ray diffraction patterns of $Ba_2(Ca_{0.75}Nb_{0.59}Ta_{0.66})O_{6-\delta}$ (a) as-prepared, (b) sample 'a' heated in 100% CO_2 at 800 °C for 7 days, and (c) sample 'a' heated in boiling water for 7 days. Insets show the selected area PXRD.

Table 2
Lattice constant and electrical conductivity of Ta-doped double perovskite-type BCN.

Composition	Cubic lattice constant (Å)			σ (S cm^{-1}) medium					
	As-prepared	CO_2 treated	H_2O treated	T (°C)	A	B	C	D	E
$Ba_2(Ca_{0.79}Nb_{0.66}Ta_{0.55})O_{6-\delta}$	8.373(2)	8.374(2)	8.388(2)	450	2.6×10^{-4}	5.8×10^{-5}	4.6×10^{-4}	2.3×10^{-4}	4.8×10^{-4}
				600	5.2×10^{-4}	2.0×10^{-4}	6.1×10^{-4}	3.3×10^{-4}	5.1×10^{-4}
$Ba_2(Ca_{0.75}Nb_{0.59}Ta_{0.66})O_{6-\delta}$	8.408(1)	8.385(3)	8.366(3)	450	1.2×10^{-4}	3.9×10^{-5}	2.5×10^{-4}	1.3×10^{-4}	2.2×10^{-4}
				600	2.3×10^{-4}	6.1×10^{-5}	2.5×10^{-4}	1.6×10^{-4}	2.0×10^{-4}
$Ba_2(Ca_{0.75}Nb_{0.66}Ta_{0.59})O_{6-\delta}$	8.375(1)	8.357(3)	8.376(2)	450	1.2×10^{-4}	3.9×10^{-5}	2.5×10^{-4}	1.3×10^{-4}	2.2×10^{-4}
				600	2.3×10^{-4}	6.1×10^{-5}	2.5×10^{-4}	1.6×10^{-4}	2.0×10^{-4}

A = air; B = dry N_2; C = N_2 + H_2O (24 °C); D = N_2 + D_2O (24 °C); E = H_2 + H_2O (24 °C).

days. The electrical conductivity in D_2O containing N_2 was found to be lower than that of mediums containing H_2O, suggesting that the charge carrier in humidified atmospheres are protons (especially below 600 °C). Among the three compounds investigated in the present study, $Ba_2(Ca_{0.79}Nb_{0.66}Ta_{0.55})O_{6-\delta}$ showed the highest proton conductivity of 4.8×10^{-4} S cm^{-1} at 1 MHz and 400 °C in wet N_2 or H_2, which is about one and half orders of magnitude lower than that of CO_2 unstable BCY and slightly higher than other double perovskite-type structure HT-SSPCs.

2. Experimental

2.1. Synthesis of Ta-doped BCN

The double perovskite oxides with nominal chemical formula of $Ba_2(Ca_{0.75}Nb_{0.59}Ta_{0.66})O_{6-\delta}$, $Ba_2(Ca_{0.75}Nb_{0.66}Ta_{0.59})O_{6-\delta}$ and $Ba_2(Ca_{0.79}Nb_{0.66}Ta_{0.55})O_{6-\delta}$ were prepared by employing solid-state (ceramic) reaction in air using appropriate amounts of high purity powder materials, such as $Ba(NO_3)_2$ (99+%, Alfa Aesar), $CaCO_3$ (99%, Fisher Scientific), Nb_2O_5 (99.5%, Alfa Aesar), and Ta_2O_5 (99.85%, Alfa Aesar). The desired amount of 2-propanol was added to these starting powder materials in a zirconia bowl and was ball milled (Pulverisette, Fritsch, Germany) for 6 h at 200 rpm using zirconia balls with an intermediate change in rotation direction every hour to ensure proper mixing. The powders were then dried and sintered in air at 1000 °C for 12 h in a clean alumina crucible. The resulting mixture was ball milled using 2-propanol again for about 6 h; then pressed into pellets (~1 cm diameter, ~2 cm thick) using isostatic pressure of about 8 MPa. The pressed pellets were sintered in air at 1500 °C for 24 h. The pellets were then ball milled

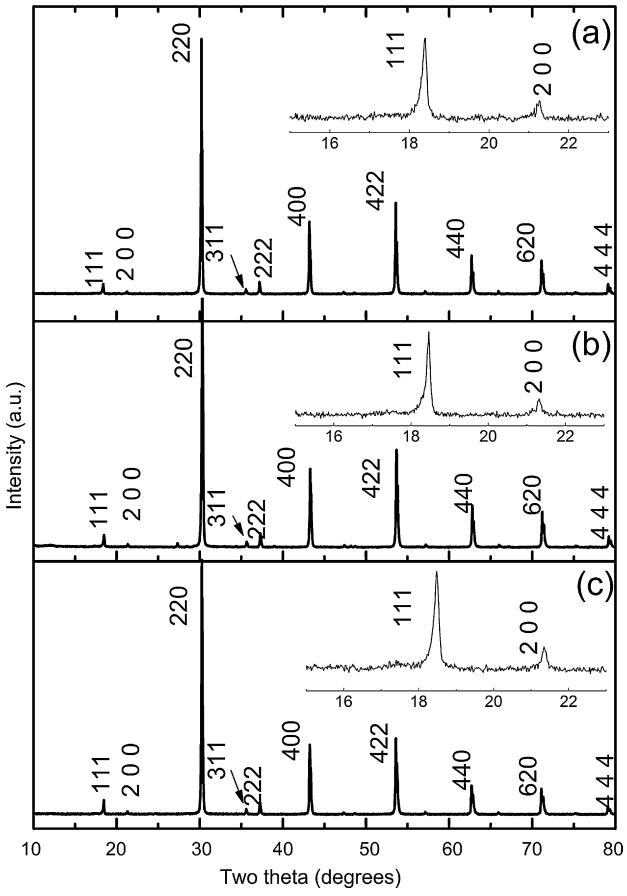

Fig. 3. Powder X-ray diffraction patterns of $Ba_2(Ca_{0.75}Nb_{0.66}Ta_{0.59})O_{6-\delta}$ (a) as-prepared, (b) sample 'a' heated in 100% CO_2 at 800 °C for 7 days, and (c) sample 'a' heated in boiling water for 7 days. Insets show the selected area PXRD.

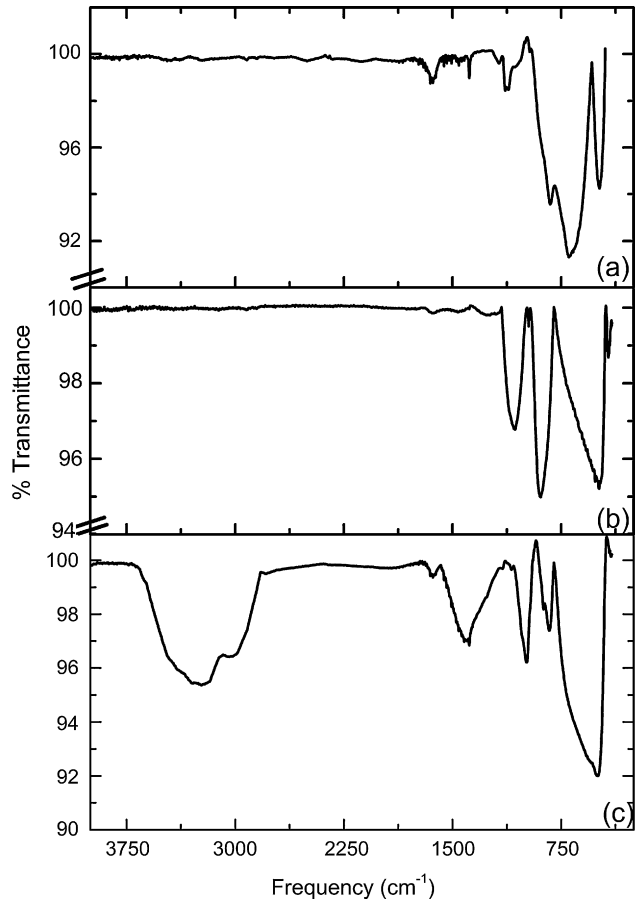

Fig. 4. FTIR spectra of $Ba_2(Ca_{0.79}Nb_{0.66}Ta_{0.55})O_{6-\delta}$ (a) as-prepared, (b) sample 'a' heated in boiling water for 7 days, and (c) sample 'a' heated in 100% CO_2 at 800 °C for 7 days. Evidently, the IR spectra of samples 'a' and 'b' are the same, suggesting the absence of carbonate formation, and sample 'c' shows a peak due to the OH group.

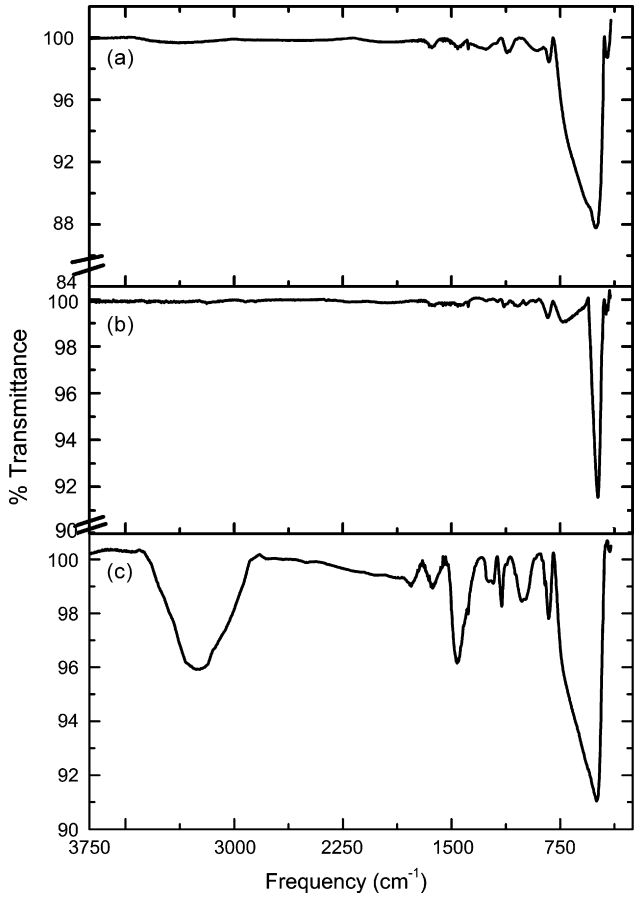

Fig. 5. FTIR spectra of $Ba_2(Ca_{0.75}Nb_{0.59}Ta_{0.66})O_{6-\delta}$ (a) as-prepared, (b) sample 'a' heated in boiling water for 7 days, and (c) sample 'a' heated in 100% CO_2 at 800 °C for 7 days. We see clearly that the IR spectra of samples 'a' and 'b' are the same, suggesting the absence of carbonate formation, and sample 'c' shows a peak due to the OH group.

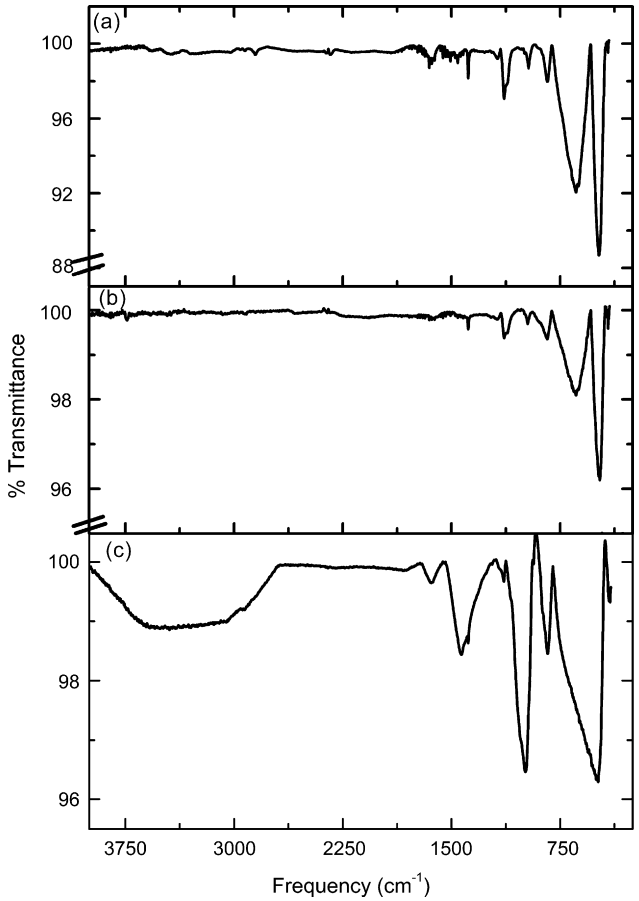

Fig. 6. FTIR spectra of $Ba_2(Ca_{0.75}Nb_{0.66}Ta_{0.59})O_{6-\delta}$ (a) as-prepared, (b) sample 'a' heated in boiling water for 7 days, and (c) sample 'a' heated in 100% CO_2 at 800 °C for 7 days. We see clearly that the IR spectra of samples 'a' and 'b' are the same, suggesting the absence of carbonate formation, and sample 'c' shows a peak due to the OH group.

into a powder for powder X-ray characterization (PXRD) using a Bruker D8 powder X-ray diffractometer (Cu Kα, 40 kV; 40 mA) at room temperature with a 2θ step scan width of 0.02 and a counting time of 6 s. The lattice constant was determined from the PXRD data by method of least squares. The chemical stability under CO_2 (at 800 °C) and boiling H_2O environment was determined on powder samples for 7 days. The resultant products were examined by PXRD.

Scanning electron microscopy (SEM) (Philips XL30 SEM) was used to study the morphology of the as-prepared and water treated samples, as well as samples after electrical measurements in $D_2O + N_2$. A gold layer was sputtered for the SEM measurements. Thermogravimetric analysis (TGA) was performed for as-prepared, CO_2 and H_2O treated materials in the temperature range 25–900 °C using a Netzsch 449C Simultaneous Thermal Analyzer in a N_2 atmosphere (5 °C min^{-1}). Further characterization involves Fourier transform infrared spectroscopy (FTIR) using a NEXUS 470 FT-IR Spectrometer. Before FTIR measurements, the KBr powder was kept continuously at about 100 °C in a vacuum oven.

2.2. Determination of electrical conductivity

Electrical conductivity measurements using Pt electrodes were performed in air, dry N_2, dry H_2 and wet N_2, wet H_2 and D_2O saturated N_2. Pt paste (Heraeus Inc., LP A88-11S, Germany) was applied using a paintbrush to both sides of the sintered pellets and cured at 900 °C for 1 h in air to remove the organic binders. Pt wires were attached to the surface of the pellet using a spring-loaded contact, which served as a current collector. The cell was heated to the desired temperature in the range 300–800 °C using a Barnstead tubular furnace (model no. 21100) and held at constant temperature prior to each measurement for a minimum of 2 h and a maximum of 48 h. The AC impedance (Solartron Electrochemical Impedance Spectroscopy; SI model no. 1260, 100 mV; 0.01 Hz to 7 MHz) was used to determine the conductivity. A two-probe electrochemical cell was employed for the electrical characterization. The conductivity of each sample was measured by subsequent heating and cooling cycles. The desired pH_2O was obtained by holding the water at selected temperature (24, 60 and 80 °C) and using N_2 as a carrier gas.

3. Results and discussion

3.1. PXRD, FTIR and TGA characterization

Fig. 1 shows the powder X-ray diffraction patterns of as-prepared, CO_2 treated (800 °C for 7 days) and water boiled (7 days) $Ba_2(Ca_{0.79}Nb_{0.66}Ta_{0.55})O_{6-\delta}$. We indexed all the observed diffraction lines based on a cubic double perovskite ($A_2B_2O_6$)-like cell with a lattice constant of $a \sim 2a_p$ (where a_p is a simple perovskite cell of about 4 Å). Table 1 gives the indexed PXRD pattern of $Ba_2(Ca_{0.79}Nb_{0.66}Ta_{0.55})O_{6-\delta}$ in three atmospheres. Similar PXRD

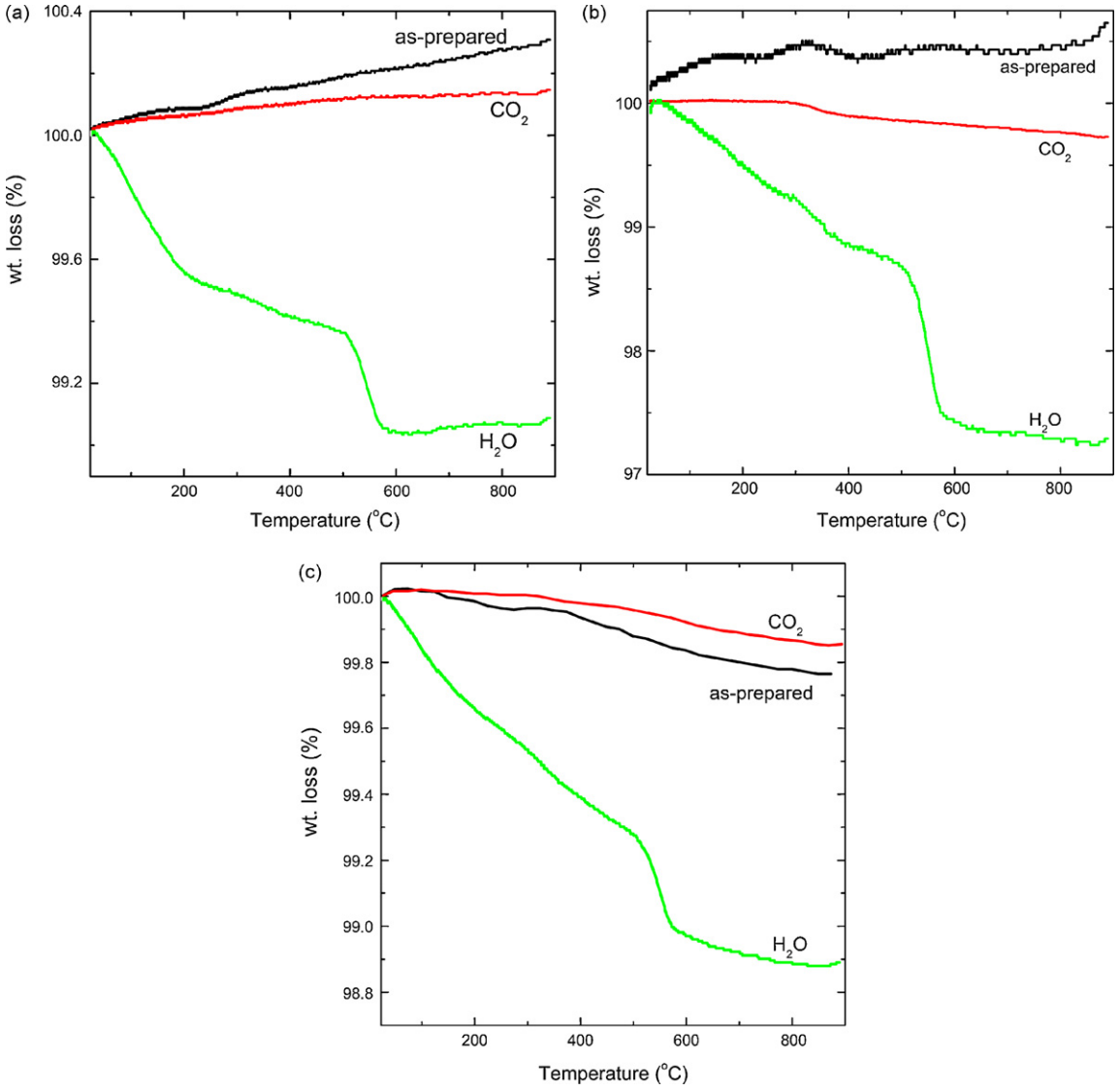

Fig. 7. TGA curves of as-prepared, water boiled and 100% CO_2 treated at 800 °C (a) $Ba_2(Ca_{0.79}Nb_{0.66}Ta_{0.55})O_{6-\delta}$, (b) $Ba_2(Ca_{0.75}Nb_{0.59}Ta_{0.66})O_{6-\delta}$ and (c) $Ba_2(Ca_{0.75}Nb_{0.66}Ta_{0.59})O_{6-\delta}$.

patterns were observed for $Ba_2(Ca_{0.75}Nb_{0.59}Ta_{0.66})O_{6-\delta}$ (Fig. 2, Table S1—supporting information) and $Ba_2(Ca_{0.75}Nb_{0.66}Ta_{0.59})O_{6-\delta}$ (Fig. 3, Table S2—supporting information). The lattice parameters were found to be comparable to those of the double perovskite-like structure, for e.g., $Ba_3Ca_{1.18}Nb_{1.82}O_{9-\delta}$ (a = 8.4106 Å) [43]. Unlike BCY, we see that the presently investigated double perovskite-like structure was retained after CO_2 (Figs. 1b, 2b and 3b) and water treatment (Figs. 1c, 2c and 3c). The cubic lattice constant of CO_2

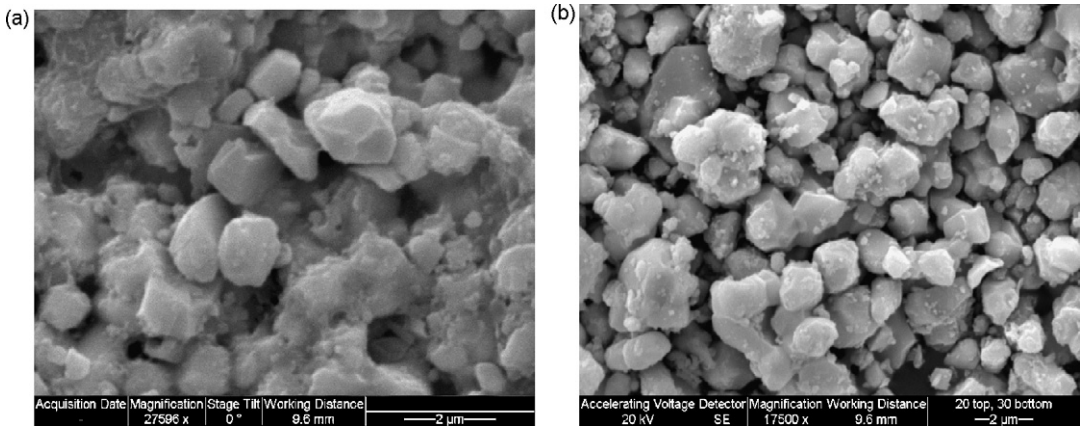

Fig. 8. SEM images of (a) as-prepared and (b) water treated $Ba_2(Ca_{0.79}Nb_{0.66}Ta_{0.55})O_{6-\delta}$.

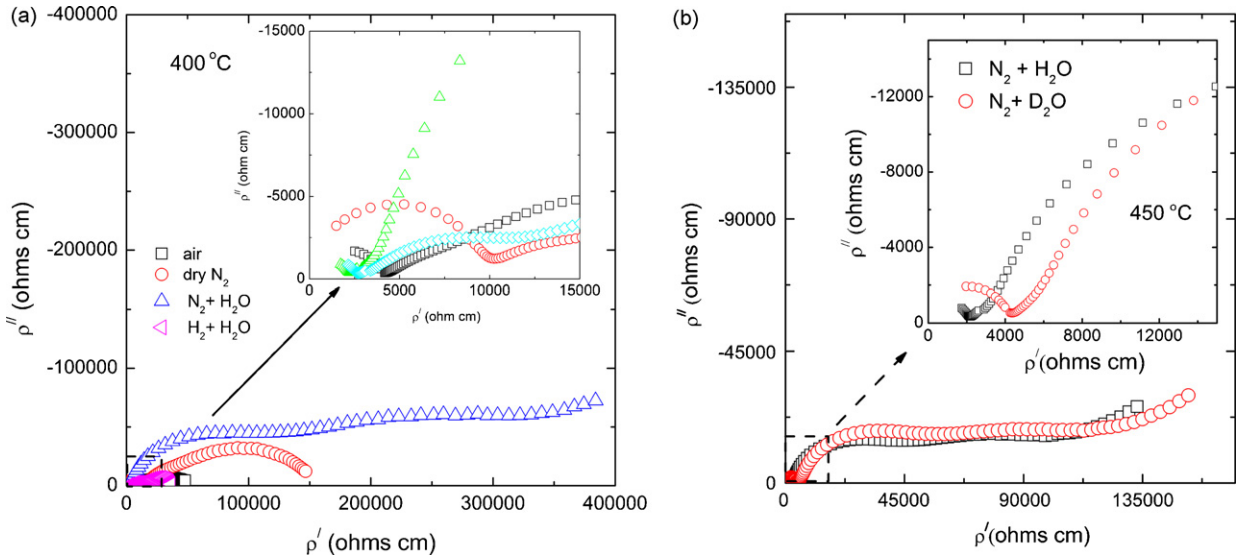

Fig. 9. Typical AC impedance plots of $Ba_2(Ca_{0.79}Nb_{0.66}Ta_{0.55})O_{6-\delta}$ (a) air, dry N_2, wet N_2, and H_2 at 400 °C. A large contribution due to grain-boundary and electrode effects at low-frequencies, and very small bulk contribution at the high-frequency region (inset). (b) $N_2 + H_2O$ (kept at 24 °C) and $N_2 + D_2O$ (kept at 24 °C) at 450 °C.

and water treated samples was found to be comparable to that of the corresponding as-prepared sample (Table 2). The absence of carbonate formation was further confirmed from the FTIR spectroscopy characterization.

Figs. 4–6 show the FTIR spectra of as-prepared, CO_2 and water treated $Ba_2(Ca_{0.79}Nb_{0.66}Ta_{0.55})O_{6-\delta}$, $Ba_2(Ca_{0.75}Nb_{0.59}Ta_{0.66})O_{6-\delta}$ and $Ba_2(Ca_{0.75}Nb_{0.66}Ta_{0.59})O_{6-\delta}$, respectively. We see that as-prepared and CO_2 reacted samples exhibit similar FTIR spectrum. There was no any peak observed due to carbonate at about 1700 cm^{-1}. Furthermore, TGA study showed no significant weight change up to 900 °C for all the CO_2 treated materials, confirming the absence of $BaCO_3$ and other potential carbonate, for e.g., $CaCO_3$ (Fig. 7). Accordingly, the presently investigated materials exhibit excellent chemical stability in CO_2.

TGA analysis of water boiled $Ba_2(Ca_{0.79}Nb_{0.66}Ta_{0.55})O_{6-\delta}$ showed a weight loss of 1.12% in the temperature range of 25–900 °C, which was attributed to the loss of water (OH group) (Fig. 7a). Schober and coworkers [36,37] and others [42] had reported similar weight loss for water treated BCY and BCN. The uptake of water in the oxygen deficient double perovskites can be explained using Eq. (1). A similar result was reported for numerous acceptor-doped metal oxides possessing perovskite-type structure, including La-doped BCY [19], $BaCe_{0.5}Zr_{0.35}Sc_{0.1}Zn_{0.05}O_{3-\delta}$ [37] and $Sr_6Ta_2O_{11}$ [44]. The amount of water uptake appears to be related to the oxide ion vacancy concentration and the nature of A-and B-site cations.

3.2. SEM characterization

SEM characterization was used to evaluate the change in microstructure after the materials were treated with boiling water. Fig. 8 shows the SEM images of as-prepared and water treated $Ba_2(Ca_{0.79}Nb_{0.66}Ta_{0.55})O_{6-\delta}$. A similar SEM image was observed for the other two members of the series of compounds investigated in the present work. We see clearly that the water boiled $Ba_2(Ca_{0.79}Nb_{0.66}Ta_{0.55})O_{6-\delta}$ have a slight growth of particles compared to the as-prepared samples. Furthermore, the SEM images show a homogeneous size distribution of particles after a water treatment

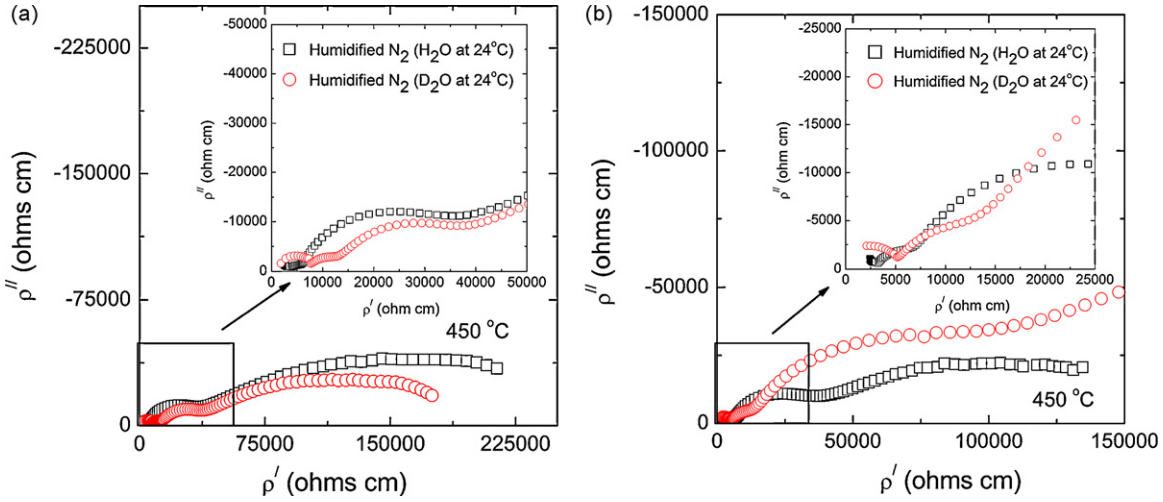

Fig. 10. Typical AC impedance plots for (a) $Ba_2(Ca_{0.75}Nb_{0.59}Ta_{0.66})O_{6-\delta}$ and (b) $Ba_2(Ca_{0.75}Nb_{0.66}Ta_{0.59})O_{6-\delta}$ in humidified N_2 and deuterium water humidified N_2 at 450 °C.

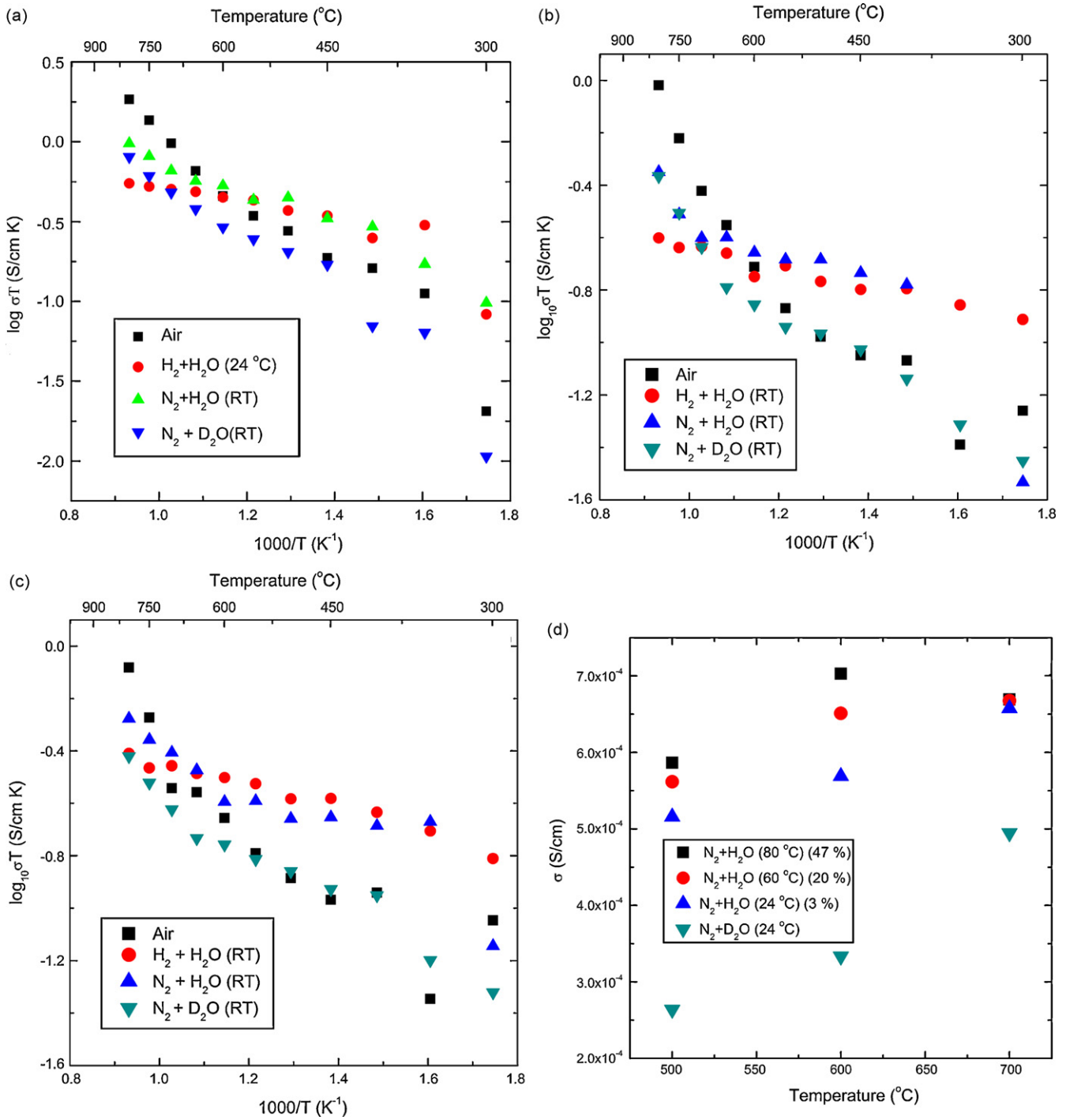

Fig. 11. Electrical conductivity of (a) $Ba_2(Ca_{0.79}Nb_{0.66}Ta_{0.55})O_{6-\delta}$, (b) $Ba_2(Ca_{0.75}Nb_{0.59}Ta_{0.66})O_{6-\delta}$, and (c) $Ba_2(Ca_{0.75}Nb_{0.66}Ta_{0.59})O_{6-\delta}$ in air, wet N_2, H_2, and deuterium containing N_2. In (d), we show the variation of proton conductivity of sample 'a' at 500, 600 and 700 °C as a function of pH_2O and D_2O.

3.3. AC impedance spectroscopy and proton conductivity

The AC impedance study showed obviously the contributions due to bulk, grain-boundary, and electrode effects in the frequency range of 0.01 Hz to 7 MHz. However, these contributions vary significantly according to the chemical compositions of the compounds as well as temperature and atmospheres of the surrounding environment. Fig. 9 shows typical ac impedance plots of $Ba_2(Ca_{0.79}Nb_{0.66}Ta_{0.55})O_{6-\delta}$ in various atmospheres. Measurements were made during the heating and cooling cycles and the shape of the impedance plots was found to be highly reproducible. We see a bulk, grain-boundary and electrode contributions at high, intermediate and low-frequency regions. A similar impedance plot was reported for several perovskite-type proton conducting alkaline cerates, niobates and zirconates in literature [25,38]. A spike in the high frequency region (commonly observed at above 1 MHz) is an artifact of the equipment. Raj et al. have reported similar data for doped $LaGaO_3$, using the same Solartron impedance frequency analyzer for electrical characterization [45]. However, in the present work, the high frequency spike at above 1 MHz was

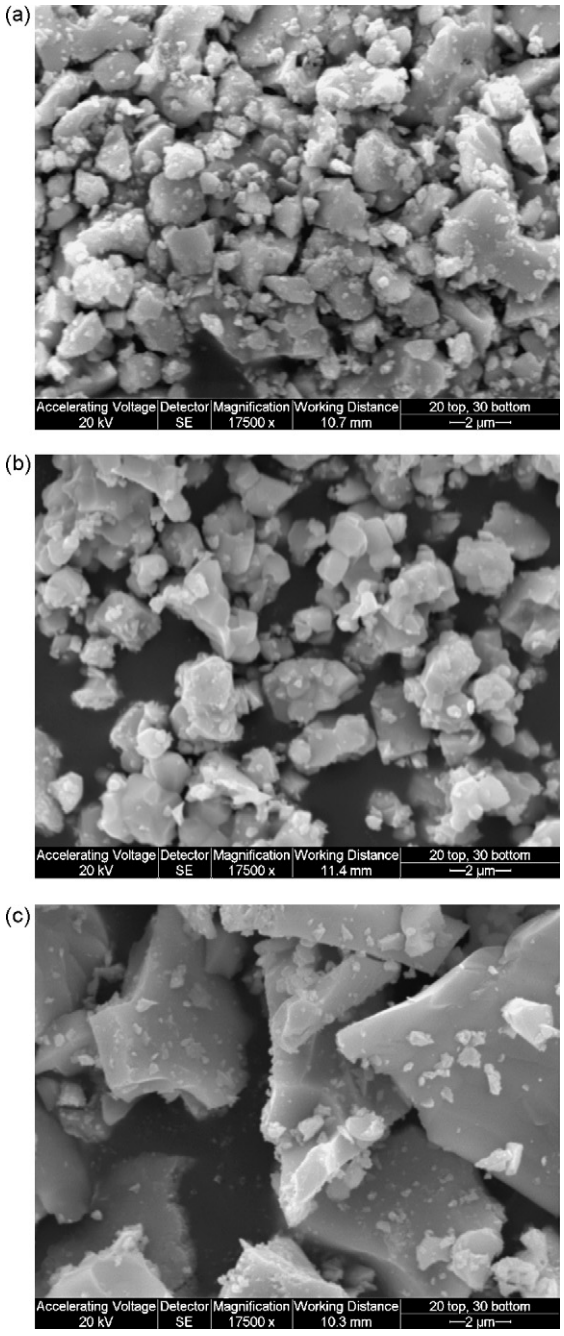

Fig. 12. SEM images of (a) $Ba_2(Ca_{0.75}Nb_{0.59}Ta_{0.66})O_{6-\delta}$, (b) $Ba_2(Ca_{0.75}Nb_{0.66}Ta_{0.59})O_{6-\delta}$ and (c) $Ba_2(Ca_{0.79}Nb_{0.66}Ta_{0.55})O_{6-\delta}$ after electrical measurements in D_2O.

found to vary with the total impedance of the sample. For highly conducting samples, this artifact was not visible clearly. Fig. 10 shows the AC impedance plots of $Ba_2(Ca_{0.75}Nb_{0.59}Ta_{0.66})O_{6-\delta}$ and $Ba_2(Ca_{0.75}Nb_{0.66}Ta_{0.59})O_{6-\delta}$ in $D_2O + N_2$ at 450 °C.

The detailed analysis of impedance plots appears to be very complex in the present system because we could not clearly distinguish the bulk, grain-boundary and electrode effects over the entire range of temperatures and various atmospheres. The 1 MHz real part value (especially, at above 500 °C) has been taken uniformly to determine the conductivity of samples in all the atmospheres (air, dry N_2, wet N_2, H_2). It is also important to mention that Norby and coworkers used the 10 kHz value to determine the bulk proton conductivity of Ca-doped $LaNbO_4$ [46]. Furthermore, Feng and Goodenough [47] were considered 13 MHz value (at above 600 °C) as a bulk resistance to determine bulk oxide ion conductivity of Sr + Mg-doped $LaGaO_3$. The aforementioned arguments justify use of a fixed frequency impedance value to determine the ionic conductivity of solid electrolytes, exhibiting proton and oxide ion conduction.

Fig. 11 shows the Arrhenius plots for the electrical conductivity data of $Ba_2(Ca_{0.79}Nb_{0.66}Ta_{0.55})O_{6-\delta}$, $Ba_2(Ca_{0.75}Nb_{0.59}Ta_{0.66})O_{6-\delta}$, and $Ba_2(Ca_{0.75}Nb_{0.66}Ta_{0.59})O_{6-\delta}$ in air, wet N_2 and wet H_2. At low temperatures (below 600 °C) the conductivity in wet N_2 and wet H_2 was found to be an order of magnitude higher than ambient air. An opposite effect was observed at high temperatures (600–800 °C). The data obtained during the heating and cooling runs fall on the same line, suggesting equilibrium conductivity behavior. In dry N_2 and dry H_2 atmospheres, a slightly lower conductivity was observed compared to that of air over the investigated temperature range, indicating the p-type (hole) electronic conduction. Norby and coworkers observed a similar behavior under wet atmospheres for proton-conducting acceptor doped perovskite-type $BaBO_3$ (B = Pr, Tb, Th) [48]. The decrease in the electrical conductivity in wet atmosphere has been explained due to p-type electronic conduction or oxide ion conduction [46,48]. Several researchers were proposed that the increase in the electrical conductivity in wet atmosphere (below 600 °C) is mainly because of proton conduction [11,12,18,19,46,48].

Among the three compounds investigated in the present study, the $Ba_2(Ca_{0.79}Nb_{0.66}Ta_{0.55})O_{6-\delta}$ shows the highest electrical conductivity of 4.8×10^{-4} S cm^{-1} at 400 °C in wet N_2 or H_2 (Table 2), which is an order of magnitude higher than the recently reported 1% Ca-doped $LaNbO_4$ at 10 kHz [46]. The activation energy for electrical conduction was found to be 0.1–0.14 eV in wet N_2 and wet H_2 in the temperature range of 450–650 °C. A similar value has been observed for the fast proton conducting Ca-doped $LaNbO_4$ at the high temperature region [46]. The existence of proton conduction in the oxide ion deficient perovskites can be descried using Eq. (1). Furthermore, the electrical conductivity was found to increase with increasing water vapour partial pressure (pH_2O), confirming the charge carriers are protons in the investigated perovskites (Fig. 11(d)). This was further confirmed by the slight decrease in the electrical conductivity in $D_2O + N_2$ (Figs. 9–11) which can be explained using the defect equilibrium reaction.

$$D_2O_{(g)} + V_O^{\bullet\bullet} + O_O^x \rightarrow 2OD_O^{\bullet} \quad (2)$$

(where $OD_O^{\bullet}$ represents deuterium attached to the lattice oxygen). In Fig. 12, we show the SEM images of $Ba_2(Ca_{0.75}Nb_{0.59}Ta_{0.66})O_{6-\delta}$, $Ba_2(Ca_{0.75}Nb_{0.66}Ta_{0.59})O_{6-\delta}$ and $Ba_2(Ca_{0.79}Nb_{0.66}Ta_{0.55})O_{6-\delta}$ after electrical measurements in $D_2O + N_2$. For this measurement, Pt electrodes were removed and the remaining pellet was crushed into powder. Interestingly, the microstructure was found to be similar to that of the water boiled sample (Fig. 8b).

Fig. 13 compares the proton conductivity of $Ba_2(Ca_{0.79}Nb_{0.66}Ta_{0.55})O_{6-\delta}$ with other HT-SSPCs reported in literature [11,26–29,42,49,50]. Interestingly, the presently investigated Ta-doped BCN, $Ba_2(Ca_{0.79}Nb_{0.66}Ta_{0.55})O_{6-\delta}$ exhibits about an order of magnitude higher conductivity than that of $Sr_3CaZr_{0.5}Ta_{1.5}O_{8.75}$ [49], and $Sr_{5.92}Ta_{2.08}O_{11.12}$ (wet O_2) [44], but, one and half orders of magnitude lower compared to polycrystalline CO_2 unstable BCY [26]. Further research will be directed towards new A-site substitution in Ta-doped BCN to increase proton conductivity while still retaining the chemical stability in CO_2 containing atmospheres as well as in a high level of humidity at elevated temperatures.

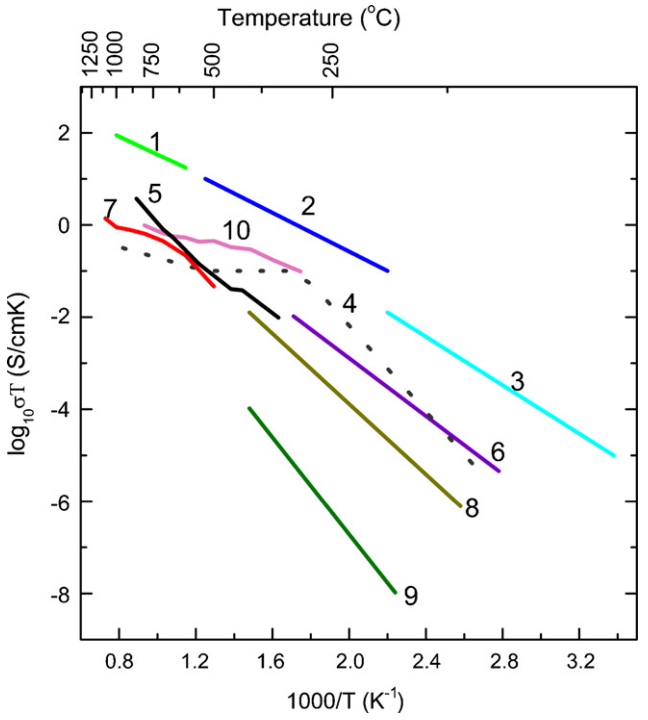

Fig. 13. Comparison of proton conductivity of $Ba_2(Ca_{0.79}Nb_{0.66}Ta_{0.55})O_{6-\delta}$ in wet N_2 with other HT-SSPCs. (1) $BaCe_{0.9}Y_{0.1}O_3$ [26], (2) single-crystal Y:$BaCeO_3$ [11], (3) $Ba_3Ca_{1+x}Nb_{(2-x)}O_{9-\delta}$ ($x = 0.18$) [33], (4) $Sr_3CaZr_{0.5}Ta_{1.5}O_{8.75}$ [49], (5) $Sr_{5.92}Ta_{2.08}O_{11.12}$ (wet O_2) [44], 6) $Sr_2(Sc_{1+x}Nb_{2-x})O_6$ [50], (7) $La_{0.99}Ca_{0.01}NbO_4$ [46], (8) $Sr_2(Ga_{1+x}Nb_{2-x})O_{6-\delta}$ ($x = 0.1$) [32], (9) $Sr_2(Nd_{1+x}Nb_{2-x})O_{6-\delta}$ ($x = 0.05$) [35], and (10) $Ba_2(Ca_{0.79}Nb_{0.66}Ta_{0.55})O_{6-\delta}$ (present work).

4. Conclusions

In summary, powder X-ray diffraction (PXRD) studies showed the formation of double perovskite-like $Ba_2(Ca_{0.75}Nb_{0.59}Ta_{0.66})O_{6-\delta}$, $Ba_2(Ca_{0.75}Nb_{0.66}Ta_{0.59})O_{6-\delta}$ and $Ba_2(Ca_{0.79}Nb_{0.66}Ta_{0.55})O_{6-\delta}$. The PXRD of CO_2 treated and water boiled samples was found to be same as the as-prepared samples, suggesting a long-term stability against chemical reaction with CO_2 and humidified conditions. The electrical conductivity of Ta-doped BCN perovskites was found to vary with surrounding atmosphere. Below 600 °C, the bulk proton conductivity in wet N_2 and wet H_2 was found to be higher compared to in air and in dry N_2 and dry H_2. However, an opposite trend was observed at high temperatures due to p-type electronic conduction. The electrical conductivity was found to be decreased in D_2O compared to that of H_2O which clearly confirmed that the investigated compounds exhibit proton conduction in wet atmospheres which was consistent with water uptake in lattice (confirmed by TGA and FTIR). Among the compounds investigated in the present work, $Ba_2(Ca_{0.79}Nb_{0.66}Ta_{0.55})O_{6-\delta}$ shows the highest proton conductivity of 4.8×10^{-4} S cm^{-1} at 400 °C in wet N_2 or H_2 and is comparable to those of other HT-SSPCs reported in the literature.

Acknowledgements

We thank the Natural Sciences and Engineering Research Council (NSERC) of Canada and the Canada Foundation for Innovation (CFI) for the financial support. We also thank Dr. George K.H. Shimizu at the Department of Chemistry, University of Calgary, for proving the TGA facility.

Appendix A. Supplementary data

Supplementary data associated with this article can be found, in the online version, at doi:10.1016/j.jpowsour.2008.09.110.

References

[1] P. Costamagna, S. Srinivasan, J. Power Sources 102 (2001) 242–252.
[2] L. Qingfeng, R. He, J.-A. Gao, J.O. Jensen, N.J. Bjerrum, J. Electrochem. Soc. 150 (2003) A1599–A1605.
[3] A. Heinzel, V.M. Barragan, J. Power Sources 84 (1999) 70–74.
[4] L. Qingfeng, R. He, J.O. Jensen, N.J. Bjerrum, Chem. Mater. 15 (2003) 4896–4915.
[5] G. Alberti, M. Casciola, Solid State Ionics 145 (2001) 3–16.
[6] R. Savinell, E. Yeager, D. Tryk, U. Landau, J. Wainright, D. Weng, K. Lux, M. Litt, C. Rogers, J. Electrochem. Soc. 141 (1994) L46–L48.
[7] M. Doyle, S.K. Choi, G. Proulx, J. Electrochem. Soc. 147 (2000) 34–37.
[8] L. Qingfeng, H.A. Hjuler, C. Hasiotis, J.K. Kallitsis, C.G. Kontoyannis, N.J. Bjerrum, Electrochem. Solid-State Lett. 5 (2002) A125–A128.
[9] W.A. England, M.G. Cross, A. Hamnett, P.J. Wiseman, J.B. Goodenough, Solid State Ionics 1 (1980) 231–249.
[10] Ph. Colomban (Ed.), Proton Conductors—Solids, Membranes and Gels-materials and Devices, Cambridge University Press, Cambridge, 1992.
[11] K.D. Kreuer, Solid State Ionics 97 (1997) 1–15.
[12] K.D. Kreuer, Annu. Rev. Mater. Res. 33 (2003) 333–359.
[13] H. Iwahara, Y. Asakura, K. Katahira, M. Tanaka, Solid State Ionics 168 (2004) 299–310.
[14] G. Alberti, M. Casciola, Annu. Rev. Mater. Rev. 33 (2003) 129–154.
[15] H. Iwahara, H. Uchida, K. Morimoto, J. Electrochem. Soc. 137 (1990) 462–465.
[16] H. Uchida, N. Maeda, H. Iwahara, Solid State Ionics 11 (1983) 117–124.
[17] K.D. Kreuer, E. Schijnherr, J. Maier, Solid State Ionics 70/71 (1994) 278–284.
[18] R. Glo¨ckner, M.S. Islam, T. Norby, Solid State Ionics 122 (1999) 145–156.
[19] A. Kruth, R.A. Davies, M.S. Islam, J.T.S. Irvine, Chem. Mater. 19 (2007) 1239–1248.
[20] C.W. Tanner, A.V. Virkar, J. Electrochem. Soc. 143 (1996) 1386–1389.
[21] S.V. Bhide, A.V. Virkar, J. Electrochem. Soc. 146 (1999) 2038–2044.
[22] S.V. Bhide, A.V. Virkar, J. Electrochem. Soc. 146 (1999) 4386–4392.
[23] H. Matsumoto, Y. Kawasaki, N. Ito, M. Enoki, T. Ishihara, Electrochem. Solid-State Lett. 10 (2007) B77–B80.
[24] A.K. Azad, J.T.S. Irvine, Solid State Ionics 178 (2007) 635–640.
[25] K.H. Ryu, S.M. Haile, Solid State Ionics 125 (1999) 355–367.
[26] K. Katahira, Y. Kohchi, T. Shimura, H. Iwahara, Solid State Ionics 138 (2000) 91–98.
[27] E. Fabbri, A.D. Epifanio, E.D. Bartolomeo, S. Licoccia, E. Traversa, Solid State Ionics 179 (2008) 558–564.
[28] E. Fabbri, D. Pergolesi, A.D. Epifanio, E.D. Bartolomeo, G. Balestrino, S. Licoccia, E. Traversa, Energy Environ. Sci. 1 (2008) 355–359.
[29] S. Tao, J.T.S. Irvine, J. Solid State Chem. 180 (2007) 3493–3503.
[30] A.K. Azad, J.T.S. Irvine, Solid State Ionics 179 (2008) 678–682.
[31] A.K. Azad, C. Savaniu, S. Tao, S. Dual, P. Holtappels, R.M. Ibberson, J.T.S. Irvine, J. Mater. Chem. 18 (2008) 3414–3418.
[32] K.C. Liang, A.S. Nowick, Solid State Ionics 61 (1993) 77–81.
[33] K.C. Liang, Y. Du, A.S. Nowick, Solid State Ionics 69 (1994) 117–120.
[34] A.S. Nowick, Y. Du, Solid State Ionics 77 (1995) 137–146.
[35] A.S. Nowick, Y. Du, K.C. Liang, Solid State Ionics 125 (1999) 303–311.
[36] F. Krug, T. Schober, Solid State Ionics 92 (1996) 297–302.
[37] T. Schober, F. Krug, W. Schilling, Solid State Ionics 97 (1997) 369–373.
[38] S. Valkenberg, H.G. Bohn, W. Schilling, Solid State Ionics 97 (1997) 511–515.
[39] T. Schober, J. Friedrich, Solid State Ionics 136–137 (2000) 161–165.
[40] W. Wang, A.V. Virkar, J. Electrochem. Soc. 150 (2003) A92–A97.
[41] W. Wang, A.V. Virkar, J. Electrochem. Soc. 150 (2004) A1565–A1571.
[42] J.T.S. Irvine, D.J.D. Corcoran, J.C. Vazquez, Solid State Ionics 152–153 (2002) 749–757.
[43] E. Zimmer, K. Scharf, T. Mono, J. Friedrich, T. Schober, Solid State Ionics 97 (1997) 505–509.
[44] I. Animitsa, T. Norby, S. Marion, R. Glo¨ckner, A. Neiman, Solid State Ionics 145 (2001) 357–364.
[45] E.S. Raj, S.J. Skinner, J.A. Kilner, Solid State Ionics 176 (2005) 1097–1101.
[46] P. Haugsrud, T. Norby, Nat. Mater. 5 (2006) 193–196.
[47] M. Feng, J.B. Goodenough, Eur. J. Solid State Inorg. Chem. 31 (1994) 663–672.
[48] K.A. Furøy, R. Haugsrud, M. Hänsel, A. Magrasó, T. Norby, Solid State Ionics 178 (2007) 461–467.
[49] D.J.D. Corcoran, J.T.S. Irvine, Solid State Ionics 145 (2001) 307–313.
[50] A.S. Nowick, K.C. Liang, Solid State Ionics 129 (2000) 201–207.